iScience

Article

Exploring reductive stress as a regulation approach for *Pseudomonas Aeruginosa* biofilm

Graphical abstract

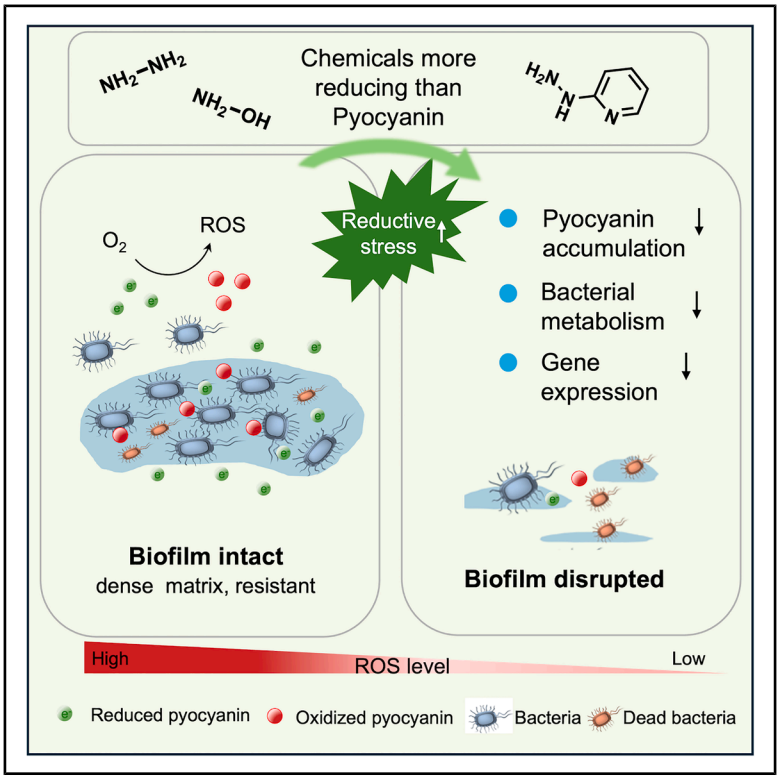

Highlights

- Reductive stress provides a strategy for regulating *P.aeruginosa* biofilms
- Effective reductants feature lower redox potentials compared to pyocyanin
- Hydrazine treatment leads to decreased accumulation of pyocyanin in biofilm
- Hydroxylamine is a lead candidate with balanced efficacy and cytocompatibility

Authors

Jie Liu, Youzhi Li, Kairuo Yan, Jinghua Han, Ziqi Wu, Ying Li

Correspondence

yingli0e@hku.hk

In brief

Health sciences; Pharmaceutical science; Microbiology

Liu et al., 2025, iScience *28*, 113973
December 19, 2025
https://doi.org/10.1016/j.isci.2025.113973

CellPress

iScience

CellPress
OPEN ACCESS

Article

Exploring reductive stress as a regulation approach for *Pseudomonas Aeruginosa* biofilm

Jie Liu,[1,2] Youzhi Li,[1] Kairuo Yan,[1] Jinghua Han,[1,2] Ziqi Wu,[1] and Ying Li[1,2,3,*]
[1]Department of Chemistry, The University of Hong Kong, Hong Kong, China
[2]Laboratory for Synthetic Chemistry and Chemical Biology Limited, New Territories, Hong Kong, China
[3]Lead contact
*Correspondence: yingli0e@hku.hk
https://doi.org/10.1016/j.isci.2025.113973

SUMMARY

Pseudomonas aeruginosa (*P. aeruginosa*) biofilms pose substantial challenges in clinical settings due to their resistance to conventional antibiotic treatments. This study investigated the influence of reductive stress on the formation and eradication of *P. aeruginosa* biofilms. A series of redox-active compounds were employed to assess their impact on both biofilm development and disruption. Among them, hydrazine (HZ) showed potent activity. Mechanistic studies revealed that these compounds suppressed pyocyanin production and impaired bacterial metabolic activity. A structure-activity relationship analysis highlighted hydroxylamine (HA) as a promising candidate, owing to its favorable balance between efficacy and cytotoxicity. Notably, quantitative reverse transcription polymerase chain reaction (RT-qPCR) analysis of HA-treated *P. aeruginosa* suggested inhibition of matrix biosynthesis, quorum sensing, and oxidative stress defenses. This study provides insights into biofilm management by targeting the redox environment, offering potential strategies for the development of redox-based therapies to combat biofilm-associated infections.

INTRODUCTION

Pseudomonas aeruginosa (*P. aeruginosa*) is an opportunistic human pathogen that develops difficult-to-treat biofilms, posing significant threat to immunocompromised individuals, cystic fibrosis patients, and those with chronic wounds.[1] Biofilms formed by *P. aeruginosa* contribute to the physiological attributes that enable the bacteria to evade conventional antibiotic treatments, allowing for resistance to develop.[2] In medical scenarios, the accumulation of biofilms can foul implants, trigger chronic immune responses, and complicate treatment outcomes.[3] Thus, understanding the factors that regulate biofilm formation and maturation is of critical importance.

Biofilms are structured communities of bacteria that are encased within a self-generated matrix of extracellular polymeric substances (EPS), including extracellular DNAs (eDNAs) and proteins.[4,5] These eDNAs and proteins originate partially from lysed and dead bacteria within the community. On one hand, they can serve as traps for traditional antibiotics, thus mitigating their antibacterial effects on live bacteria within the biofilm matrix. On the other hand, these eDNAs and proteins offer a network for electron transfer, which is important for quorum sensing within biofilms.[6,7] While biofilms dampen and minimize the impact of typical antibiotics, this dense matrix also leads to slow growth of bacteria due to less available oxygen and nutrients deep within the biofilm core.[8,9] Hence, bacterial communities have collectively evolved a few strategies to survive in this challenging environment.[10]

One of bacteria's survival strategies involves the production and release of redox-active molecules into biofilms. These molecules transfer electrons from the carbon-rich biofilm core through the biopolymer to oxygen.[10] Oxygen serves as a terminal oxidant at the outer region of the biofilm. These redox-active molecules include but not limited to pyocyanin, one of the major phenazines found in biofilms.[11] Pyocyanin (PYO) plays a dual and tightly regulated role in *P. aeruginosa* biofilms. In the hypoxic core of mature biofilms, PYO functions as an essential extracellular electron shuttle, facilitating anaerobic respiration and maintaining redox homeostasis under oxygen-limited or nutrient-deprived conditions.[12,13] However, in aerobic regions of the biofilm, pyocyanin undergoes redox-mediated interactions with molecular oxygen, facilitating the generation of reactive oxygen species (ROS) that promoting oxidative damage to bacterial subpopulations.[14,15] To balance these opposing effects, *P. aeruginosa* employs spatial compartmentalization, where reduced PYO accumulates in anoxic niches, while oxidative damage is mitigated in aerobic regions via antioxidant defences, such as katA-encoded catalase.[16] Additionally, quorum sensing regulators (lasR, rhlR) control PYO biosynthesis in response to cell density and environmental stress, ensuring that PYO production aligns with metabolic demand.[17] Recent findings also suggest that PYO-induced cell death may serve as a programmed sacrifice mechanism, releasing nutrients for surrounding cells and contributing to metabolic heterogeneity within the biofilm community. Perturbing electron transfer pathways via small molecular metabolites and biomacromolecules might

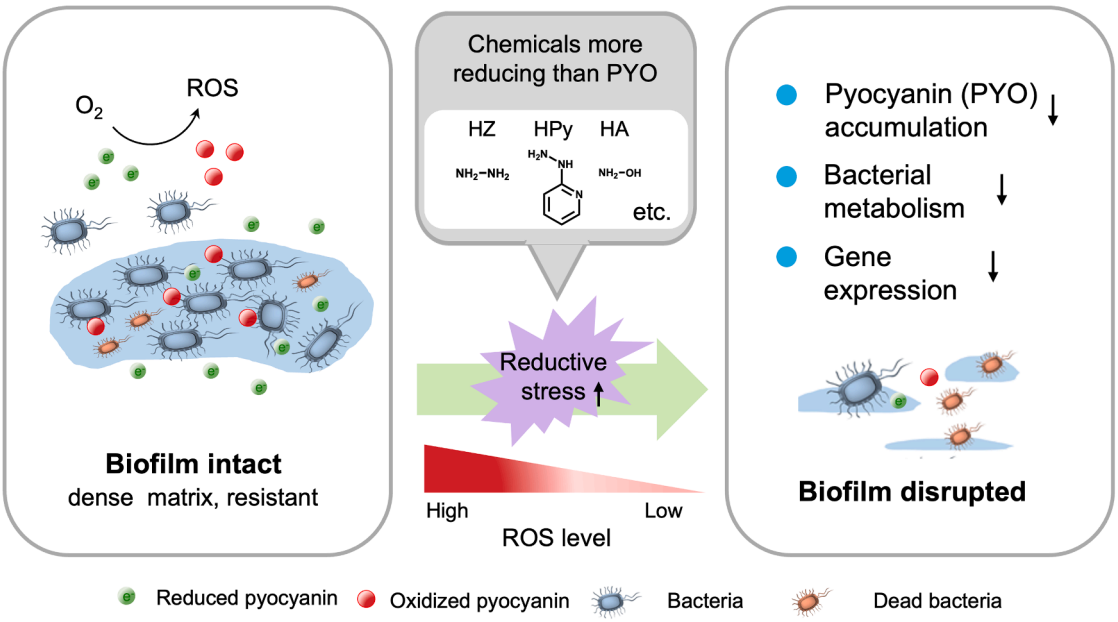

Scheme 1. Reductive stress as a strategy to regulate *P. aeruginosa* biofilms

serve as a feasible approach to regulate biofilm formation and elicit biofilm eradication.

Research on the use of antioxidants for biofilm regulation focuses on leveraging their ability to nullify ROS and alleviate oxidative stress within bacterial communities.[18] Antioxidants, including vitamin C, *N*-acetylcysteine (NAC), flavonoids, melatonin, and dithiothreitol (DTT), have demonstrated utility in inhibiting biofilm formation and enhancing the susceptibility of biofilms to antimicrobial treatments. By lowering oxidative stress, these compounds can interfere with bacterial quorum sensing, hinder the production of EPS, and disrupt biofilm integrity. DTT is known to disrupt biofilms primarily by breaking disulfide bonds present in proteins that constitute the biofilm matrix.[19,20] In contrast, sodium ascorbate removes ROS, which plays a vital role in biofilm signaling pathways.[21]

Research on pro-oxidants, also known as anti-reductants, for biofilm regulation exploits their capacity to induce oxidative stress by increasing ROS levels within biofilms. Agents such as hydrogen peroxide,[22,23] sodium hypochlorite,[23,24] nitric oxide,[25] and metal ions like copper[26] and silver[27] have been used to disrupt biofilm formation and promote biofilm dispersal. These compounds generate oxidative damage to bacterial cells and the extracellular matrix, compromising biofilm structure, and interfering with bacterial signaling processes.[28]

Despite of the advances mentioned above, a more systematic approach is needed to select and screen antioxidants and pro-oxidants for more effective biofilm regulation.[29] Here, we screen a range of redox reagents and discover suitable biofilm redox regulators. Rationally designed derivatives of the candidate with the best biofilm regulation properties from the array of screened molecules were further investigated via biomass change, bacteria regrowth capacity, and mammalian cell cytotoxicity studies. Moreover, the underlying mechanisms by which these biofilm regulators exert their antibiofilm effects were further elucidated (Scheme 1).

RESULTS

Redox potential correlates with biofilm inhibition efficacy

We initially selected a range of chemicals with varying redox potentials, emphasizing more on the reduction spectrum. The molecular structures and their corresponding redox potentials are listed in Figure 1. These chemicals feature redox potentials ranging from −0.75 V to 0.83 V vs. NHE,[30–39] spanning across pyocyanin, an important redox signaling molecule for biofilm formation and maturation. We utilized agar plates to screen the selected chemicals and access their impact on biofilm formation. The agar plates were formulated with increasing concentrations of the candidates displayed in Figure 1. *P. aeruginosa* PAO1 was inoculated onto the corresponding agar plates and incubated at 37°C for 24 h. The size of colony-based biofilm was used to evaluate the impact of candidates on *P. aeruginosa* PAO1 biofilm formation (Figure 2). Persistent biofilm formation was observed in sodium ascorbate, and sodium sulfite, even at a high concentration of 100 mM. In sharp contrast, the other four chemicals completely suppressed the biofilm formation at concentrations equal to or above 12.5 mM, except for 2-mecaptoethanol that yielded a faint colony-shape biofilm at this concentration. While a slightly more obvious colony showed after the treatment with 6.25 mM DTT, this concentration of hydrazine treatment afforded no observable biofilm formation. These results indicated a positive correlation between the biofilm inhibition efficacy and the redox potentials of the tested compounds. We further hypothesize that chemicals with redox potentials more negative than that of pyocyanin tend to exhibit

A

	Chemical name	Redox potential (pH=7)
1	Hydrazine hydrate	-750 mV
2	Dithiothreitol (DTT)	−330 mV
3	Tris(2-carboxyethyl)phosphine (TCEP)	−290 mV
4	2-Mercaptoethanol	−260 mV
	Pyocyanin (PYO)	-32 mV
5	Sodium ascorbate	280 mV
6	Na_2SO_3	830 mV

B

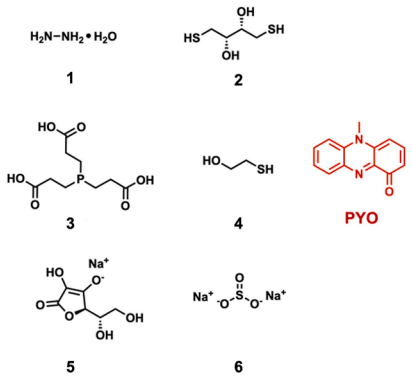

Figure 1. Selected chemicals for biofilm regulation

(A) Redox potentials,[30–39] and (B) molecular structures of the selected chemicals.

enhanced inhibitory effects on *P. aeruginosa* PAO1 biofilm formation. To further test this correlation, we included D-glucose, a common reducing sugar with a redox potential of approximately −0.1 V.[40] However, unlike other reducing agents, D-glucose also serves as a carbon source readily metabolized by bacteria. As such, it deviates from the observed trend and exhibited only moderate inhibitory activity at a high concentration (100 mM) (supplemental information, Figure S1). In contrast, its non-metabolizable analog, L-glucose, failed to show any noticeable biofilm inhibition at all tested concentrations. These findings suggest that metabolic utilization can confound the redox-based inhibitory effects and underscore the importance of considering both redox potential and metabolic reactivity when evaluating biofilm inhibition mechanisms.

Based on preliminary evidence that certain reducing agents inhibited *P. aeruginosa* biofilm formation, we proceeded to explore potential mechanisms of action. Initially, we accessed the impact of these compounds on planktonic viability. Chemicals with redox potentials more negative than that of pyocyanin exhibited stronger bactericidal activity against free-living cells (supplemental information, Figure S2), suggesting that the biofilm formation inhibition started with impacting individual

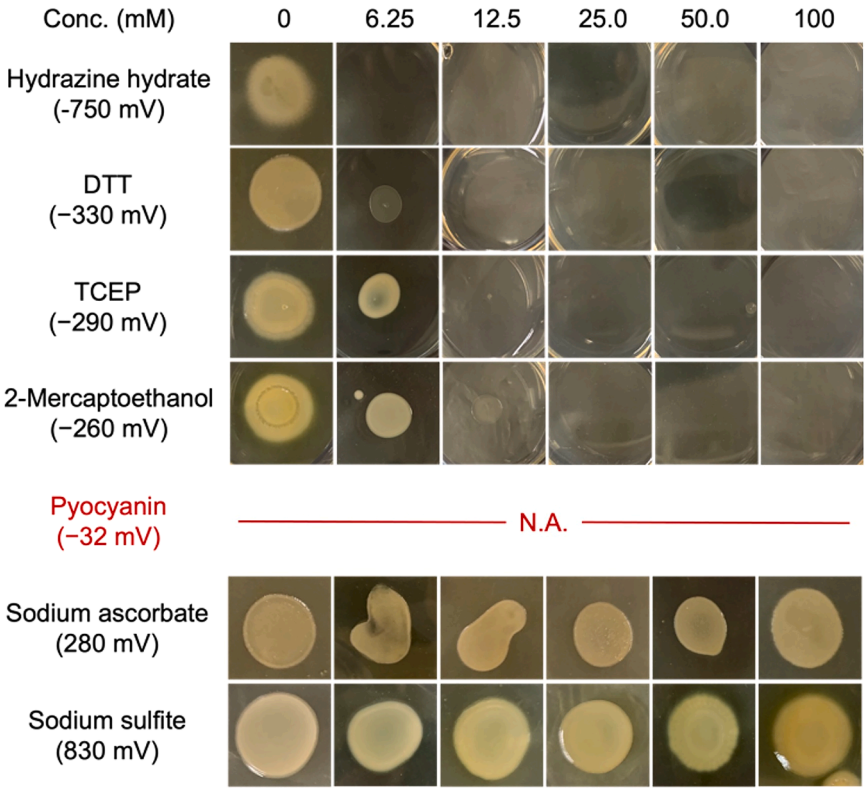

Figure 2. Agar assay of *Pseudomonas aeruginosa* PAO1 biofilm formation upon treatment with selected chemicals

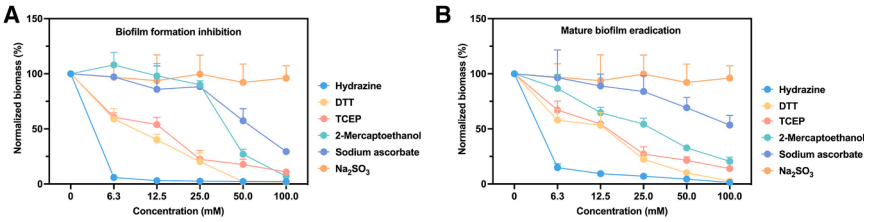

Figure 3. Quantification of inhibition and eradication of biofilm via crystal violet assay

(A) Biofilm formation inhibition effect of chemicals of interest in a dose-dependent manner.

(B) Mature biofilm eradication effect of chemicals of interest in a dose-dependent manner. Data are represented as mean ± SD (n = 3).

bacteria. To further quantify the antibiofilm effects of the tested compounds, we employed crystal violet staining to measure biomass (supplemental information, Figure S3). The assay was conducted under two distinct conditions: (1) inhibition of biofilm formation, where chemicals were incubated with free bacteria and the biomass formation was monitored at the conclusion of the experiment; (2) eradication of mature biofilm, where chemicals were introduced to established biofilm and the remaining biomass was evaluated at the end. These two scenarios represent the two important stages fighting against biofilm.

The results of the biomass formation inhibition and eradication, as measured by the crystal violet assay, were summarized in Figure 3. Across the concentration range of 0–100 mM, sodium sulfite showed negligible effects on both biofilm formation and eradication. Despite observable colony biofilm formation at high concentrations of sodium ascorbate (Figure 2), the crystal violet assay suggested significant biofilm biomass reduction, achieving more than 60% inhibition at 100 mM (Figure 3). The eradication effects, while slightly compromised, were sustained at about 50%, likely due to the complex structure of the preformed mature biofilm. Different from sodium ascorbate and sodium sulfite, DTT, TCEP, and 2-mercaptoethanol share redox potentials lower than pyocyanin with a decreasing trend (DTT < TCEP < 2-mercaptoethanol < pyocyanin). They demonstrated biofilm regulation behavior correlated to their redox potential, with 2-mecaptoethanol exhibiting the lowest biofilm inhibition and eradication capability among the three. Despite having similar redox potentials, DTT outperformed 2-mercaptoethanol, likely due to its unique structure, DTT contains two thiol groups in a rigid ring enabling efficient intramolecular redox cycling and deeper penetration into the biofilm, whereas 2-mercaptoethanol, bearing a single thiol group, undergoes slower intermolecular oxidation, which limits its redox efficiency in dense biofilm matrices. Specifically, DTT and TCEP afforded relatively similar dose-dependent biofilm inhibition and eradication performance, with a minimal biofilm inhibitory concentration ($MBIC_{50}$) and a minimal biofilm eradication concentration ($MBEC_{50}$) at around 12.5 mM. 2-mercaptoethanol demonstrated higher efficiency in mature biofilm eradication ($MBIC_{50} \approx$ 25.0 mM) compared to biofilm formation inhibition ($MBEC_{50}$ > 25.0 mM). The mature biofilm eradication effect steadily increased as the concentration increased. However, no obvious biofilm formation inhibition effect was observed up to 25.0 mM. In sharp contrast to all the other chemicals, hydrazine exhibited significantly strong inhibition and eradication effects on biofilms at a concentration of 6.25 mM. It is important to highlight that hydrazine features the lowest redox potential among all the chemicals used in this assay. To further probe the observed correlation between redox potential and antibiofilm efficacy, we additionally evaluated D-glucose and its non-metabolizable isomer, L-glucose. While D-glucose exhibited measurable antibiofilm activity, L-glucose showed no significant effect on either biofilm formation or eradication across all tested concentrations (supplemental information, Figure S4).

Antibiofilm activity of reducing agents is linked to ROS modulation

To investigate whether the antibiofilm activity of the reducing agents is mediated via modulation of intracellular ROS levels, we performed DCFDA (2′,7′-dichlorofluorescin diacetate) staining to quantify ROS production following chemical treatments. As shown in Figure 4, the concentration-dependent ROS decreasing trend resembled that of biomass revealed by crystal violet assay. This clear correlation observed between ROS level and biofilm biomass indicated that these reducing agents might disrupt biofilm integrity by imposing strong reductive stress. In contrast, agents with weaker antibiofilm effects (sodium ascorbate and sodium sulfite) showed minimal reduction of ROS levels, consistent with their limited efficacy in prior biomass assays. Interestingly, treatment with high concentrations of sodium sulfite not only failed to reduce ROS levels in mature biofilms but appeared to restore ROS levels to those of untreated wild-type controls. This paradoxical effect may be attributed to sulfite-induced oxidative stress under certain conditions.[41,42] Additionally, we were intrigued by the effect of D-glucose treatment on biofilm ROS. Unexpectedly, rather than decreasing ROS levels, D-glucose led to a gradual increase in biofilm ROS (supplemental information, Figure S5). This observation implies that its biofilm-related effects are more likely associated with oxidative stress rather than reductive stress.

Structure-activity relationship of hydrazine derivatives

With the prominent inhibition effect from hydrazine (HZ), we proceeded to explore several hydrazine derivatives to explore their structure-property relationship. Hydrazine derivatives with different substitutions were selected (Figure 5A). Other than hydroxylamine (HA), all the other derivatives maintain the characteristic nitrogen-nitrogen single bond. We systematically explored the effect of single nitrogen substituted analogs, including mono-alkylated hydrazine as well as di-alkylated ones. One of the mono-alkylated hydrazine features a γ-terminal alcohol (2-hydroxylethyl hydrazine, HEH) while the other is directly conjugated with an electron deficient pyridine at the C2 position (2-hydrazinopyridine, HPy). All the di-alkylated hydrazine derivatives enjoy heterocyclic ring structures. Compared to 1-aminopiperidine (AP), 1-amino-4-methylpiperazine (AMP)

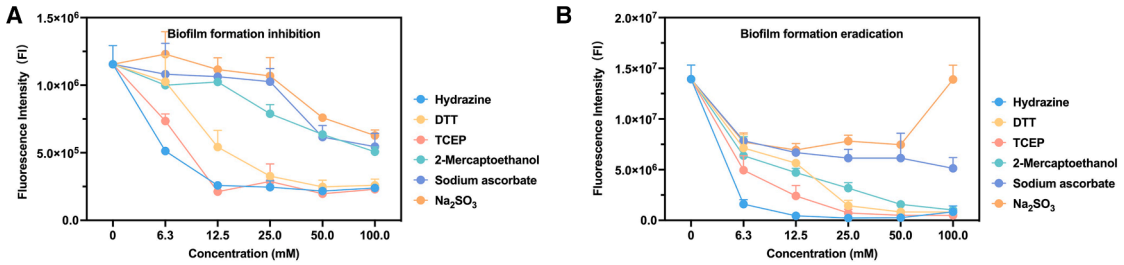

Figure 4. Measurement of ROS levels in biofilms treated with selected redundant using DCFDA (2′,7′-dichlorofluorescin diacetate) assay

(A) ROS detected during biofilm formation treated with different concentrations of selected chemicals for 48 h.

(B) ROS detected during mature biofilm eradication treated with the different concentration of selected reductant for 48 h. Data are represented as mean ± SD (n = 3).

affords an additional tertiary amine while 3-amino-3-azabicyclo[3.3.0]octane (AAO) presents a heavily constrained aliphatic skeleton frequently found in natural products and biologically active compounds.[43,44]

Prior to evaluating the effects of HZ derivatives on biofilm biomass, we first assessed their bactericidal activity against planktonic *P. aeruginosa* cells (supplemental information, Figure S6). Among the tested compounds, HZ, HPy, and HEH exhibited the strongest bactericidal effects, completely inhibiting bacterial growth at concentrations as low as 6.25 mM. HA showed moderate activity, with growth inhibition observed from 12.5 mM and above. In contrast, AAO and AP were less effective, requiring at least 25.0 mM and 50.0 mM, respectively, to achieve comparable inhibition. AAO showed minimal activity even at 100 mM. Crystal violet assays revealed overall consistent trends in antibiofilm activity but with some deviation (Figures 5B, 5C, and S7; supplemental information). HPy was the only compound that matched HZ in both biofilm formation inhibition and mature biofilm eradication, with $MBIC_{50}$ and $MBEC_{50}$ values below 6.25 mM. Although HA afforded similarly strong biofilm inhibition effect, its performance in eradication dropped to a $MBEC_{50}$ of 12.5 mM. Different from its strong tendency to inhibit free bacteria, HEH demonstrated dampened activity in biofilm inhibition and eradiation, with both $MBIC_{50}$ and $MBEC_{50}$ values

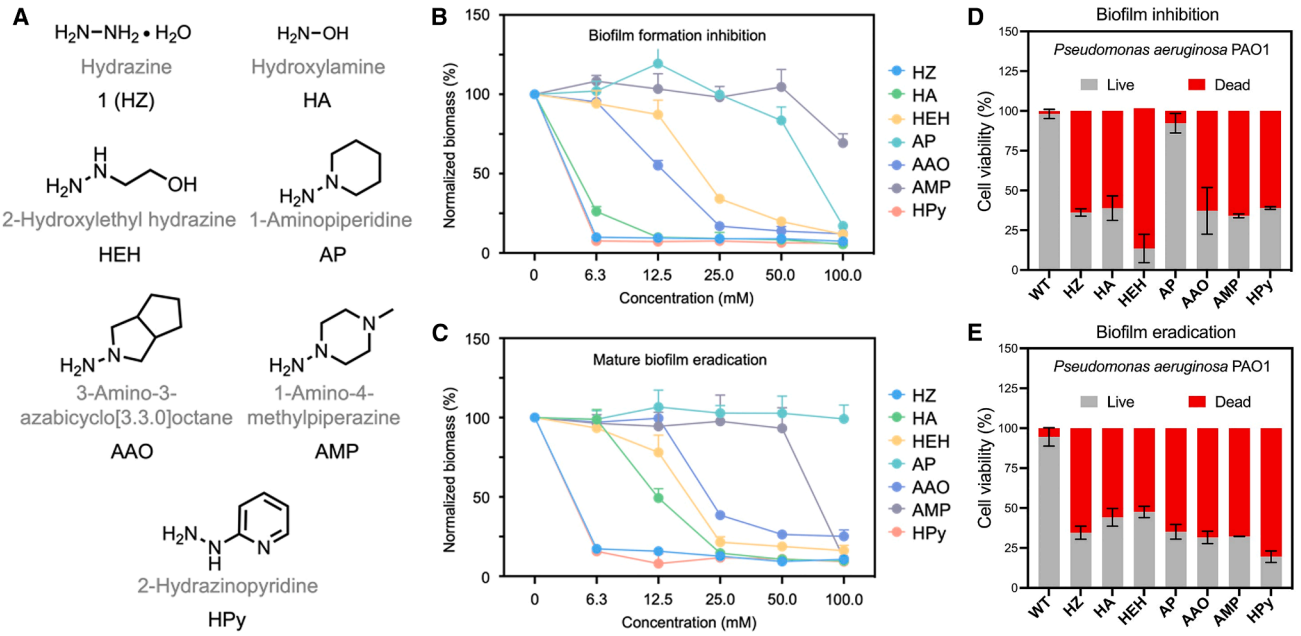

Figure 5. Evaluation of biofilm biomass and bacterial viability following treatment with hydrazine derivatives

(A) Chemical structures and names of selected hydrazine derivatives.

(B) Biofilm biomass quantified by crystal violet staining to assess inhibition of biofilm formation.

(C) Biofilm biomass quantified by crystal violet staining to assess eradication of mature biofilms.

(D) Bacterial viability during biofilm inhibition analyzed using the Live/Dead BacLight assay.

(E) Bacterial viability during biofilm eradication analyzed using the Live/Dead BacLight assay. Viability was quantified using ImageJ; data are shown as mean ± SD (n = 3).

exceeding 12.5 mM. Out of the three disubstituted hydrazine molecules, AAO showed the highest efficiency, which was comparable to HEH, a mono and linear substituted hydrazine derivative. As for AP and AMP, little negative impacts were observed on biofilm up to 50.0 mM. At 100 mM, AP inhibited biofilm formation by ~80% but failed to eradicate mature biofilms. Conversely, AMP was more effective in biofilm eradication than in inhibition, suggesting that the presence of a tertiary amine group may enhance biofilm penetration. Given the pronounced antibiofilm activity of HZ and HPy, we conducted more detailed concentration-dependent analyses to compare their performance (supplemental information, Figure S8). Both compounds exhibited comparable efficacy in biofilm inhibition and eradication, with HZ displaying slightly superior activity, particularly at lower concentrations.

To further assess the viability of biofilm-embedded cells following treatment, Live/Dead BacLight staining was performed at $MBIC_{50}$ and $MBEC_{50}$ concentrations for each compound (supplemental information, Table S1, Figures S9, S10, 5D, and 5E). All derivatives except AP resulted in a much higher level of dead bacteria in biofilm compared to the non-treated groups. Compounds with potent antibiofilm activity, such as HZ, HPy, HA, HEH, and AAO caused a substantial decrease in viable cells, consistent with their biomass-reducing effects. Conversely, AP resulted in minimal dead cells within biofilm, indicating limited impact on both planktonic cells as well as biofilm. Notably, HEH displayed the highest dead-cell staining during biofilm inhibition but the lowest during mature biofilm eradication, suggesting limited biofilm penetration capability. Together, these results highlight the structural dependence of hydrazine derivatives' antibiofilm performance, substitution patterns, and functional group characteristics jointly influencing both biomass reduction and bacterial viability within the biofilm matrix.

Hydrazine derivatives suppress bacterial metabolism and pyocyanin production

To investigate whether the antibiofilm effects of hydrazine derivatives are associated with disruption of bacterial metabolic activity, we assessed cell viability within biofilms using XTT and resazurin reduction assays after 48 h of treatment (Figures 6A–6D). Consistent with biofilm biomass measurements, the metabolic activity in early-stage biofilm formation (Figures 6A and 6C) was significantly suppressed by HZ and HPy in a concentration-dependent manner. Notably, HZ and HPy exhibited the most potent inhibitory effect, leading to near-complete loss of XTT and resazurin signals at concentrations $\geq$12.5 mM. HA, HEH, and AAO also markedly decreased metabolic activity, albeit to a slightly lesser extent. These results suggest that these chemicals led to not only biofilm accumulation disruption but also bacterial metabolic activity suppression. In mature biofilms (Figures 6B and 6D), similar trends were observed. HZ, HPy, and HA again induced substantial decrease in both XTT absorbance and resazurin fluorescence signals, indicating effective disruption of metabolic activity within preformed biofilms. In contrast, AMP exhibited limited effects on metabolic activity across the tested concentration range, consistent with their weaker biofilm eradication profiles.

To further elucidate the potential mechanisms underlying the antibiofilm activity of the tested hydrazine derivatives, we focused on the quantification of pyocyanin, a redox-active virulence factor essential for *P. aeruginosa* survival under hypoxic biofilm conditions.[11] Given the potent antibiofilm efficacy of HZ, we first examined whether HZ could be attributed to a direct chemical degradation of pyocyanin. Mass spectrometric analysis was performed to compare commercially available pyocyanin and pyocyanin extracted from wild-type *P. aeruginosa* PAO1 before and after incubation with HZ. As shown in Figure S11, neither 1.5 mM nor 3.0 mM HZ treatment at 37°C for 48 h caused detectable alterations in the characteristic m/z peaks of pyocyanin, regardless of its source. These findings indicated that HZ does not induce irreversible chemical degradation of pyocyanin under the tested conditions. Then we investigated HZ impact on pyocyanin production during biofilm formation inhibition process, as shown in Figure 6E, treatment with increasing concentrations of HZ led to a dose-dependent decrease in pyocyanin levels in both the supernatant and the biofilm fractions. However, after normalizing by the bacterial density (Figure 6F), pyocyanin levels decreased progressively in biofilm while that in supernatant remained mostly constant with the increasing HZ concentrations. The final acute increase might result from the extremely low bacteria remained in the supernatant fraction. These results implied that HZ might inhibit pyocyanin biosynthesis in the biofilm, thereby compromising the electron-shuttling capacity and survival advantage of *P. aeruginosa* in the biofilm microenvironment.

These findings support the hypothesis that the antibiofilm activity of selected hydrazine derivatives involves dual aspects: (1) direct impairment of bacterial metabolic activity within the biofilm matrix, and (2) inhibition of redox-active virulence factor (pyocyanin) production. This metabolic suppression might contribute to pyocyanin biosynthesis impairment, thereby lower bacterial viability and promote biofilm destabilization.

According to the above assays, we found that HZ and HPy exhibited prominent anti-biofilm performance. However, due to the inherent resilience of biofilms and their tendency to reform, it is critical to assess the potential of biofilm recurrence following treatment. Indeed, we conducted the biofilm reformation assay by continuously treating biofilms over a 7-day period (Figures S12 and S13). The results indicate that HPy was able to maintain its inhibitory and eradicating effects for a longer duration compared to HZ. However, by the fourth day, biofilms treated with both HZ and HPy had returned to pre-treatment levels at effective concentration, indicating that the biofilms regained their ability to reform. These findings suggest that effective biofilm control using reductants requires higher concentrations or prolonged maintenance of MBIC not only for initial inhibition but also for preventing recurrence.

Cytotoxicity assessment identifies hydroxylamine as a promising candidate

To assess the clinical translational potential of the hydrazine derivatives, their cytotoxicity toward mammalian cells was evaluated using CCK-8 assays in HEK293T cells (Figure 7). Though HZ and HPy exhibited comparable efficacy in both biofilm formation inhibition and mature biofilm eradication, they showed

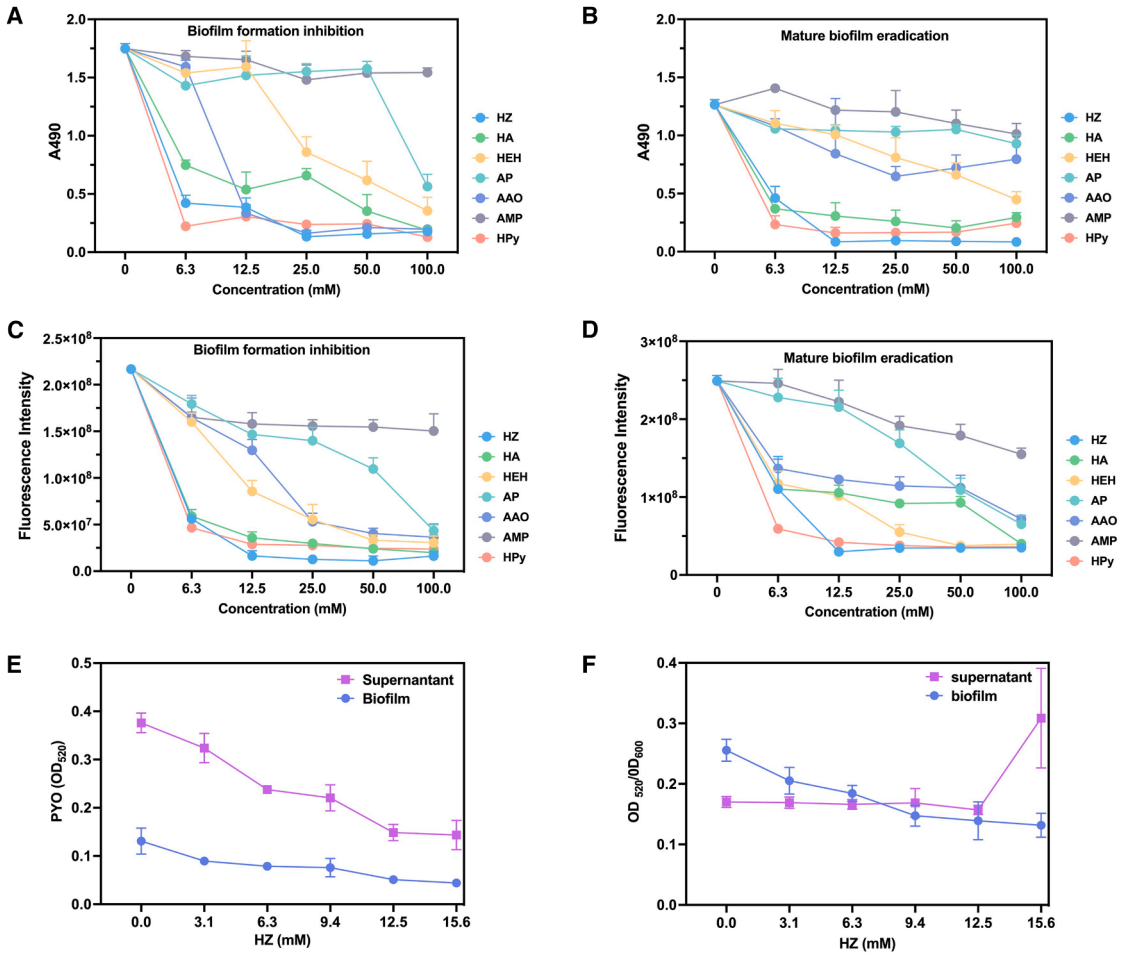

Figure 6. Elucidating the potential mechanisms underlying the antibiofilm activity of the tested hydrazine derivatives

(A) Metabolic activity of biofilms during formation, assessed by XTT assay.

(B) Metabolic activity of mature biofilms, assessed by XTT assay.

(C) Resazurin-based assessment of metabolic activity during biofilm formation.

(D) Resazurin-based assessment of metabolic activity in mature biofilms.

(E) Pyocyanin levels in the supernatant and biofilm fractions of *P. aeruginosa* PAO1 after 48 h of hydrazine treatment.

(F) The ratio of pyocyanin levels to bacterial cell density in the supernatant and within the biofilm. Data in all panels are represented as mean ± SD (n = 3).

slightly different cytotoxic profiles. Specifically, HZ demonstrated acceptable cytotoxicity (~75% cell viability) up to 1 mM while HPy exhibited a dramatic increase in cytotoxicity between 0.3 and 1 mM. Considering the MBICs of HZ and HPy being ~1.1 mM and 1.3 mM, HPy had no suitable therapeutical window, and HZ featured a very narrow window to balance cytotoxicity and its biofilm inhibition efficacy. Interestingly, HA, which exhibited moderate antibiofilm activity, demonstrated desirable biocompatibility with HEK293T cells, indicating its promise as a lead compound for further structural optimization. In contrast, HEH and AAO showed significant cytotoxicity even at their $MBIC_{50}$ concentrations. Notably, AP and AMP, despite their limited antibiofilm activity, also displayed substantial cytotoxicity at concentrations above 12.5 mM, thereby further limiting their potential as therapeutic candidates. Taken together, HA stands out as the most promising candidate, balancing moderate antibiofilm efficacy with favorable cytocompatibility. However, the $MBEC_{50}$ of HZ and HA led to less than 75% HEK293T cell viability. In another word, neither HZ nor HA afforded sufficient efficacy in biofilm formation inhibition and mature biofilm eradication within the cytocompatibility concentration range. These results highlight the importance of structural determinants in balancing antimicrobial activity and host cell compatibility. Future studies should focus on refining structure-activity-toxicity relationships to optimize the therapeutic window and improve the safety and efficacy of biofilm-targeted treatments.[45]

Hydroxylamine inhibits genes for matrix formation, quorum sensing, and stress defense

To further elucidate the mechanism underlying HA's antibiofilm activity, we analyzed the transcriptional profiles of key genes associated with exopolysaccharide biosynthesis (*pelA*, *pslA*),[46] oxidative stress response (*katA*),[47] and quorum sensing

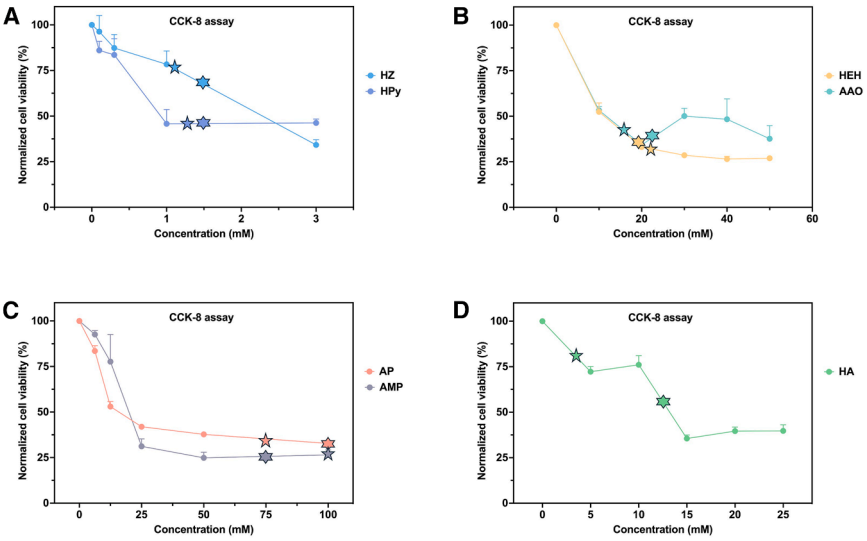

Figure 7. Cytotoxicity assessment in HEK293T cells treated with varying concentrations of hydrazine derivatives

(A) Cytotoxicity of HZ and HPy.

(B) Cytotoxicity of HEH and AAO.

(C) Cytotoxicity of AP and AMP.

(D) Cytotoxicity of HA. All data were determined by the CCK-8 assay. Data are presented as mean ± SD (n = 3). Pentagram symbols indicate the $MBIC_{50}$, while hexagram symbols represent the $MBEC_{50}$ for each compound.

regulation (*lasR*)[48] in both biofilm-embedded and planktonic *P. aeruginosa* PAO1 cells (Figure 8 and Table S2). Quantitative reverse transcription polymerase chain reaction (RT-qPCR) results revealed that HA treatment markedly suppressed *pelA* and *pslA* expression in both biofilm and planktonic states, indicating a broad inhibition of matrix polysaccharide synthesis. In parallel, *lasR* expression was consistently downregulated, suggesting that HA interferes with the Las quorum sensing circuit, which may further limit biofilm development and virulence factor production. Interestingly, *katA* expression in biofilm cells was significantly lowered, implying that HA impairs oxidative stress defense within the biofilm microenvironment, potentially increasing bacterial susceptibility to ROS. In contrast, *katA* transcription in planktonic cells remained largely unchanged, highlighting a biofilm-specific effect. Taken together, these transcriptional changes indicate that HA disrupts biofilm integrity through simultaneous suppression of matrix synthesis, quorum sensing, and oxidative stress defenses. This mode of action, combined with HA's favorable cytocompatibility, underscores its potential as a promising candidate for antibiofilm applications. Moreover, these findings support our mechanistic hypothesis that reductive stress destabilizes biofilm architecture by targeting key regulatory and structural pathways. This aligns with previous studies showing that oxidative stress tends to promote EPS synthesis as a protective response to environmental threats,[13,49,50] further emphasizing the critical role of redox imbalance in modulating biofilm physiology and resilience.

DISCUSSION

This study demonstrated reductive stress modulation as a powerful strategy to combat *P. aeruginosa* biofilms. We evaluated a panel of chemicals spanning a range of redox potentials and observed that compounds with redox potentials more negative than that of pyocyanin generally exhibited enhanced inhibitory effects on biofilm formation. Our systematic investigation of redox-active compounds highlighted that hydrazine and its derivatives, particularly, HZ and HPy, display significant antibiofilm activity. This activity stems from their interference with pyocyanin-mediated electron transfer and suppression of bacterial metabolism. A study on structure-property relationships revealed that both the substitution patterns and redox potential are critical factors influencing the efficacy of biofilm inhibition and cytocompatibility. Notably, HA demonstrated an optimal balance between antibiofilm activity and safety for mammalian cells, making it a promising candidate for further development. RT-qPCR profiling further showed that HA treatment leads to extensive transcriptional suppression of genes crucial for biofilm development (*pelA*, *pslA*), quorum sensing (*lasR*), and oxidative stress defense (*katA* in biofilms). This suggests that HA's mechanism of action includes the simultaneous disruption of structural, regulatory, and protective systems within the biofilms. These findings illuminate potential redox-based strategies for biofilm management, which could be applicable in medical devices, environmental biocontrol, and industrial settings. We envision that these reductants could be developed into anti-biofilm coatings for medical implants, including but not limited to prosthetic joints and catheters, to defer biofilm formation while polymer-based hydroxylamine materials could be designed to mitigate biofouling in industrial settings, such as waste-water treatment and processing pipelines.

To enhance our understanding of the underlying mechanisms, future research will investigate additional biofilm-related phenotypes such as bacterial motility and quorum sensing. These assays will clarify whether biofilm inhibition results directly from redox stress or involves more complex regulatory networks affected by redox imbalances. Additionally, the finding that both pro-oxidants and antioxidants can disrupt biofilms suggests a potent dual-targeting strategy. This approach would exploit the spatial redox heterogeneity[10,13] of *P. aeruginosa* biofilms: employing pro-oxidants to dismantle the oxidized outer matrix while simultaneously deploying reductants to interrupt quorum sensing and electron transport in the reduced, hypoxic core, thereby achieving synergistic efficacy.

Limitations of the study

Our study has several limitations that should be acknowledged. First, all experiments were conducted *in vitro* using the standard laboratory strain *P. aeruginosa* PAO1. The efficacy of these

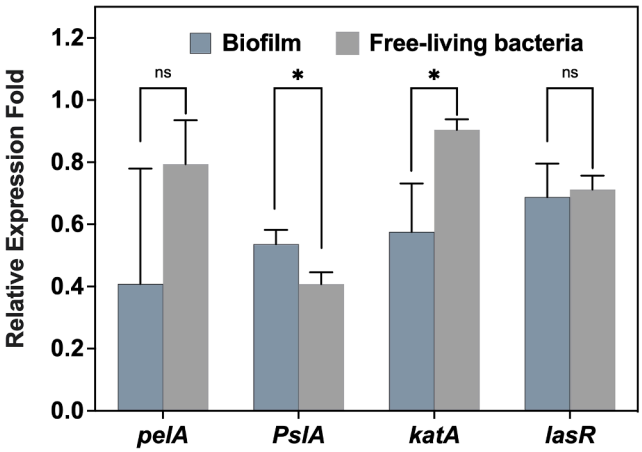

Figure 8. Quantitative reverse transcription polymerase chain reaction (RT-qPCR) analysis of gene expression

This figure shows gene expression in *P. aeruginosa* PAO1 biofilms and planktonic cells following treatment with HA, compared to untreated controls. Target genes included pelA, pslA, katA, and lasR, with rpsL used as the housekeeping gene for normalization. Data were presented as relative fold changes in expression levels. Data are presented as mean ± SD (n = 2), $^{*}p < 0.05$.

reductive agents against clinical isolates or in a more complex *in vivo* infection model remains to be determined. Second, while we identified hydroxylamine (HA) as a promising candidate due to its favorable balance of efficacy and cytotoxicity, its antibiofilm activity was less potent than that of hydrazine (HZ) or 2-hydrazinopyridine (HPy). The therapeutic window for the most effective compounds is narrow, highlighting the need for further structural optimization to enhance efficacy while minimizing host toxicity. Lastly, our mechanistic investigation focused on transcriptional changes of a few key genes; a more comprehensive approach using proteomics, transcriptomics, and or metabolomics could provide deeper insights into the global cellular response to reductive stress.

RESOURCE AVAILABILITY

Lead contact

Further information and requests for resources and reagents should be directed to and will be fulfilled by the lead contact, Ying Li (yingli0e@hku.hk).

Materials availability

This study did not generate new unique reagents.

Data and code availability

- The original data supporting the findings of this study are available from the lead contact upon reasonable request.
- This study did not generate or use new custom code.
- All other materials and resources used in this study are detailed in the key resources table or are commercially available.

ACKNOWLEDGMENTS

This work was financially supported by Hong Kong Research Grants Council (GRF 17318422, 17308925) and the Laboratory for Synthetic Chemistry and Chemical Biology under the Health@InnoHK Program launched by the Innovation and Technology Commission (Hong Kong, China). The authors gratefully acknowledge the generous gift of *Pseudomonas aeruginosa* (PAO1) bacteria line from Prof. Yongxin Li at the University of Hong Kong. The authors gratefully acknowledge the usage of plate reader in Prof. Kou Okuro's lab at the University of Hong Kong.

AUTHOR CONTRIBUTIONS

Conceptualization, Ying Li; methodology, Ying Li, J.L., Youzhi Li, and J.H.; investigation, J.L., K.Y., and Z.W.; writing—original draft, Ying Li. and J.L.; writing—review and editing, Ying Li. and J.L.; funding acquisition, Ying Li.; resources, Ying Li.; supervision, Ying Li.

DECLARATION OF INTERESTS

The authors declare no competing interests.

STAR★METHODS

Detailed methods are provided in the online version of this paper and include the following:

- KEY RESOURCES TABLE
- EXPERIMENTAL MODEL AND STUDY PARTICIPANT DETAILS
  - Bacterial strain
  - Cell line
- METHOD DETAILS
  - Agar growth assay for selected reagents against *P. aeruginosa* biofilm
  - Antimicrobial activity test for selected reagents against *P. aeruginosa*
  - Quantitation of biofilm biomass
  - DCFDA assay for biofilm ROS quantification
  - Live/Dead BacLight viability assay
  - Quantification of pyocyanin levels in biofilms treated with hydrazine
  - XTT and resazurin assays for biofilm metabolic activity
  - Cytotoxicity assay
  - RNA extraction
  - qRT-PCR
- QUANTIFICATION AND STATISTICAL ANALYSIS

SUPPLEMENTAL INFORMATION

Supplemental information can be found online at https://doi.org/10.1016/j.isci.2025.113973.

Received: November 8, 2024
Revised: August 28, 2025
Accepted: November 4, 2025
Published: November 10, 2025

REFERENCES

1. Driscoll, J.A., Brody, S.L., and Kollef, M.H. (2007). The epidemiology, pathogenesis and treatment of Pseudomonas aeruginosa infections. Drugs *67*, 351–368. https://doi.org/10.2165/00003495-200767030-00003.
2. Nickel, J.C., Ruseska, I., Wright, J.B., and Costerton, J.W. (1985). Tobramycin resistance of Pseudomonas aeruginosa cells growing as a biofilm on urinary catheter material. Antimicrob. Agents Chemother. *27*, 619–624. https://doi.org/10.1128/aac.27.4.619.
3. Cochrane, D.M., Brown, M.R., Anwar, H., Weller, P.H., Lam, K., and Costerton, J.W. (1988). Antibody response to Pseudomonas aeruginosa surface protein antigens in a rat model of chronic lung infection. J. Med. Microbiol. *27*, 255–261. https://doi.org/10.1099/00222615-27-4-255.
4. Whitchurch, C.B., Tolker-Nielsen, T., Ragas, P.C., and Mattick, J.S. (2002). Extracellular DNA Required for Bacterial Biofilm Formation. Science *295*, 1487. https://doi.org/10.1126/science.295.5559.1487.

5. Toyofuku, M., Roschitzki, B., Riedel, K., and Eberl, L. (2012). Identification of Proteins Associated with the Pseudomonas aeruginosa Biofilm Extracellular Matrix. J. Proteome Res. *11*, 4906–4915. https://doi.org/10.1021/pr300395j.

6. Wang, F., Gu, Y., O'Brien, J.P., Yi, S.M., Yalcin, S.E., Srikanth, V., Shen, C., Vu, D., Ing, N.L., Hochbaum, A.I., et al. (2019). Structure of Microbial Nanowires Reveals Stacked Hemes that Transport Electrons over Micrometers. Cell *177*, 361–369.e10. https://doi.org/10.1016/j.cell.2019.03.029.

7. Hammond, J.H., Dolben, E.F., Smith, T.J., Bhuju, S., and Hogan, D.A. (2015). Links between Anr and Quorum Sensing in Pseudomonas aeruginosa Biofilms. J. Bacteriol. *197*, 2810–2820. https://doi.org/10.1128/jb.00182-15.

8. Liu, J., Prindle, A., Humphries, J., Gabalda-Sagarra, M., Asally, M., Lee, D.-Y.D., Ly, S., Garcia-Ojalvo, J., and Süel, G.M. (2015). Metabolic co-dependence gives rise to collective oscillations within biofilms. Nature *523*, 550–554. https://doi.org/10.1038/nature14660.

9. Jo, J., Price-Whelan, A., and Dietrich, L.E.P. (2022). Gradients and consequences of heterogeneity in biofilms. Nat. Rev. Microbiol. *20*, 593–607. https://doi.org/10.1038/s41579-022-00692-2.

10. Saunders, S.H., Edmund, C., Yates, M.D., Otero, F.J., Trammell, S.A., Stemp, E.D., Barton, J.K., Tender, L.M., and Newman, D.K. (2020). Extracellular DNA promotes efficient extracellular electron transfer by pyocyanin in Pseudomonas aeruginosa biofilms. Cell *182*, 919–932.e919.

11. Dietrich, L.E.P., Price-Whelan, A., Petersen, A., Whiteley, M., and Newman, D.K. (2006). The phenazine pyocyanin is a terminal signalling factor in the quorum sensing network of Pseudomonas aeruginosa. Mol. Microbiol. *61*, 1308–1321. https://doi.org/10.1111/j.1365-2958.2006.05306.x.

12. Glasser, N.R., Kern, S.E., and Newman, D.K. (2014). Phenazine redox cycling enhances anaerobic survival in P seudomonas aeruginosa by facilitating generation of ATP and a proton-motive force. Mol. Microbiol. *92*, 399–412.

13. Schiessl, K.T., Hu, F., Jo, J., Nazia, S.Z., Wang, B., Price-Whelan, A., Min, W., and Dietrich, L.E.P. (2019). Phenazine production promotes antibiotic tolerance and metabolic heterogeneity in Pseudomonas aeruginosa biofilms. Nat. Commun. *10*, 762.

14. Das, T., and Manefield, M. (2012). Pyocyanin promotes extracellular DNA release in Pseudomonas aeruginosa. PLoS One *7*, e46718. https://doi.org/10.1371/journal.pone.0046718.

15. Meirelles, L.A., and Newman, D.K. (2018). Both toxic and beneficial effects of pyocyanin contribute to the lifecycle of Pseudomonas aeruginosa. Mol. Microbiol. *110*, 995–1010. https://doi.org/10.1111/mmi.14132.

16. Heo, Y.-J., Chung, I.-Y., Cho, W.-J., Lee, B.-Y., Kim, J.-H., Choi, K.-H., Lee, J.-W., Hassett, D.J., and Cho, Y.-H. (2010). The major catalase gene (katA) of Pseudomonas aeruginosa PA14 is under both positive and negative control of the global transactivator OxyR in response to hydrogen peroxide. J. Bacteriol. *192*, 381–390.

17. Recinos, D.A., Sekedat, M.D., Hernandez, A., Cohen, T.S., Sakhtah, H., Prince, A.S., Price-Whelan, A., and Dietrich, L.E.P. (2012). Redundant phenazine operons in Pseudomonas aeruginosa exhibit environment-dependent expression and differential roles in pathogenicity. Proc. Natl. Acad. Sci. USA *109*, 19420–19425.

18. da Cruz Nizer, W.S., Adams, M.E., Allison, K.N., Montgomery, M.C., Mosher, H., Cassol, E., and Overhage, J. (2024). Oxidative stress responses in biofilms. Biofilm *7*, 100203. https://doi.org/10.1016/j.bioflm.2024.100203.

19. Hufnagel, D.A., Price, J.E., Stephenson, R.E., Kelley, J., Benoit, M.F., and Chapman, M.R. (2018). Thiol Starvation Induces Redox-Mediated Dysregulation of Escherichia coli Biofilm Components. J. Bacteriol. *200*, e00389-17. https://doi.org/10.1128/jb.00389-17.

20. Hufnagel, D.A., DePas, W.H., and Chapman, M.R. (2014). The disulfide bonding system suppresses CsgD-independent cellulose production in Escherichia coli. J. Bacteriol. *196*, 3690–3699. https://doi.org/10.1128/jb.02019-14.

21. El-Mowafy, S.A., Shaaban, M.I., and Abd El Galil, K.H. (2014). Sodium ascorbate as a quorum sensing inhibitor of Pseudomonas aeruginosa. J. Appl. Microbiol. *117*, 1388–1399. https://doi.org/10.1111/jam.12631.

22. Mai-Prochnow, A., Lucas-Elio, P., Egan, S., Thomas, T., Webb, J.S., Sanchez-Amat, A., and Kjelleberg, S. (2008). Hydrogen Peroxide Linked to Lysine Oxidase Activity Facilitates Biofilm Differentiation and Dispersal in Several Gram-Negative Bacteria. J. Bacteriol. *190*, 5493–5501. https://doi.org/10.1128/jb.00549-08.

23. DeQueiroz, G.A., and Day, D.F. (2007). Antimicrobial activity and effectiveness of a combination of sodium hypochlorite and hydrogen peroxide in killing and removing Pseudomonas aeruginosa biofilms from surfaces. J. Appl. Microbiol. *103*, 794–802. https://doi.org/10.1111/j.1365-2672.2007.03299.x.

24. del Carpio-Perochena, A., Bramante, C.M., de Andrade, F.B., Maliza, A.G.A., Cavenago, B.C., Marciano, M.A., Amoroso-Silva, P., and Duarte, M.H. (2015). Antibacterial and dissolution ability of sodium hypochlorite in different pHs on multi-species biofilms. Clin. Oral Investig. *19*, 2067–2073. https://doi.org/10.1007/s00784-015-1431-6.

25. Cutruzzolà, F., and Frankenberg-Dinkel, N. (2016). Origin and Impact of Nitric Oxide in Pseudomonas aeruginosa Biofilms. J. Bacteriol. *198*, 55–65. https://doi.org/10.1128/jb.00371-15.

26. Dwidjosiswojo, Z., Richard, J., Moritz, M.M., Dopp, E., Flemming, H.C., and Wingender, J. (2011). Influence of copper ions on the viability and cytotoxicity of Pseudomonas aeruginosa under conditions relevant to drinking water environments. Int. J. Hyg Environ. Health *214*, 485–492. https://doi.org/10.1016/j.ijheh.2011.06.004.

27. Park, H.-J., Park, S., Roh, J., Kim, S., Choi, K., Yi, J., Kim, Y., and Yoon, J. (2013). Biofilm-inactivating activity of silver nanoparticles: A comparison with silver ions. J. Ind. Eng. Chem. *19*, 614–619. https://doi.org/10.1016/j.jiec.2012.09.013.

28. Zhang, P., Li, S., Chen, H., Wang, X., Liu, L., Lv, F., and Wang, S. (2017). Biofilm Inhibition and Elimination Regulated by Cationic Conjugated Polymers. ACS Appl. Mater. Interfaces *9*, 16933–16938. https://doi.org/10.1021/acsami.7b05227.

29. Ong, K.S., Mawang, C.I., Daniel-Jambun, D., Lim, Y.Y., and Lee, S.M. (2018). Current anti-biofilm strategies and potential of antioxidants in biofilm control. Expert Rev. Anti Infect. Ther. *16*, 855–864. https://doi.org/10.1080/14787210.2018.1535898.

30. Schröder, U. (2007). Anodic electron transfer mechanisms in microbial fuel cells and their energy efficiency. Phys. Chem. Chem. Phys. *9*, 2619–2629. https://doi.org/10.1039/b703627m.

31. Maalcke, W.J., Reimann, J., de Vries, S., Butt, J.N., Dietl, A., Kip, N., Mersdorf, U., Barends, T.R.M., Jetten, M.S.M., Keltjens, J.T., and Kartal, B. (2016). Characterization of Anammox Hydrazine Dehydrogenase, a Key N2-producing Enzyme in the Global Nitrogen Cycle. J. Biol. Chem. *291*, 17077–17092. https://doi.org/10.1074/jbc.M116.735530.

32. Creutz, C. (1981). Complexities of ascorbate as a reducing agent. Inorg. Chem. *20*, 4449–4452.

33. Cleland, W.W. (1964). Dithiothreitol, a New Protective Reagent for SH Groups. Biochemistry *3*, 480–482. https://doi.org/10.1021/bi00892a002.

34. Peng, L., Xu, X., Guo, M., Yan, X., Wang, S., Gao, S., and Zhu, S. (2013). Effects of metal ions and disulfide bonds on the activity of phosphodiesterase from Trimeresurus stejnegeri venom. Metallomics *5*, 920–927. https://doi.org/10.1039/c3mt00031a.

35. Pullela, P.K., Chiku, T., Carvan, M.J., 3rd, and Sem, D.S. (2006). Fluorescence-based detection of thiols *in vitro* and *in vivo* using dithiol probes. Anal. Biochem. *352*, 265–273. https://doi.org/10.1016/j.ab.2006.01.047.

36. Kracke, F., Vassilev, I., and Krömer, J.O. (2015). Microbial electron transport and energy conservation - the foundation for optimizing bioelectrochemical systems. Front. Microbiol. *6*, 575. https://doi.org/10.3389/fmicb.2015.00575.

37. Fruton, J.S. (1934). Oxidation-Reduction Potentials of Ascorbic Acid. J. Biol. Chem. *105*, 79–85. https://doi.org/10.1016/s0021-9258(18)75567-1.

38. Aitken, C.E., Marshall, R.A., and Puglisi, J.D. (2008). An oxygen scavenging system for improvement of dye stability in single-molecule fluorescence experiments. Biophys. J. *94*, 1826–1835. https://doi.org/10.1529/biophysj.107.117689.

39. Das, T.N., Huie, R.E., and Neta, P. (1999). Reduction potentials of SO3●-SO5●-and S4O6● 3-radicals in aqueous solution. J. Phys. Chem. A *103*, 3581–3588.

40. Vogt, S., Schneider, M., Schäfer-Eberwein, H., and Nöll, G. (2014). Determination of the pH dependent redox potential of glucose oxidase by spectroelectrochemistry. Anal. Chem. *86*, 7530–7535. https://doi.org/10.1021/ac501289x.

41. Chen, L., Tang, M., Chen, C., Chen, M., Luo, K., Xu, J., Zhou, D., and Wu, F. (2017). Efficient Bacterial Inactivation by Transition Metal Catalyzed Auto-Oxidation of Sulfite. Environ. Sci. Technol. *51*, 12663–12671. https://doi.org/10.1021/acs.est.7b03705.

42. Liang, Y., Liu, X., Chang, H., Yap, J., Sun, W., and Gao, H. (2025). Inhibitory effects of nitrite and sulfite/peroxymonosulfate on bacteria are mediated respectively through respiration and intracellular GSH homeostasis. Microbiol. Res. *290*, 127962. https://doi.org/10.1016/j.micres.2024.127962.

43. Oka, M., Matsumoto, Y., Hirooka, K., and Suzuki, T. (2000). Synthesis of 1-azabicyclo [3.3. 0] octane derivatives and their effects as piracetam-like nootropics. Chem. Pharm. Bull. *48*, 1121–1124.

44. Sokolenko, Y.M., Ostapchuk, E.N., Artemenko, A., and Grygorenko, O.O. (2017). An approach to 3-oxa-7-azabicyclo [3.3. 0] octanes–bicyclic morpholine surrogates. Synthesis *49*, 3112–3117.

45. Miret-Casals, L., Baelo, A., Julián, E., Astola, J., Lobo-Ruiz, A., Albericio, F., and Torrents, E. (2018). Hydroxylamine derivatives as a new paradigm in the search of antibacterial agents. ACS Omega *3*, 17057–17069.

46. Hassan Al-Fhdawi, A.A., and Rabee, A.M. (2023). Influence pH on virulence genes of Pseudomonas aeruginosa analyzed by RT-PCR method. Arab Gulf J. Sci. Res. *42*, 280–289. https://doi.org/10.1108/agjsr-10-2022-0244.

47. Pezzoni, M., Tribelli, P.M., Pizarro, R.A., López, N.I., and Costa, C.S. (2016). Exposure to low UVA doses increases KatA and KatB catalase activities, and confers cross-protection against subsequent oxidative injuries in Pseudomonas aeruginosa. Microbiology (Read.) *162*, 855–864. https://doi.org/10.1099/mic.0.000268.

48. García-Diéguez, L., Diaz-Tang, G., Marin Meneses, E., Cruise, V., Barraza, I., Craddock, T.J.A., and Smith, R.P. (2023). Periodically disturbing biofilms reduces expression of quorum sensing-regulated virulence factors in Pseudomonas aeruginosa. iScience *26*, 106843. https://doi.org/10.1016/j.isci.2023.106843.

49. da Cruz Nizer, W.S., Allison, K.N., Adams, M.E., Vargas, M.A., Ahmed, D., Beaulieu, C., Raju, D., Cassol, E., Howell, P.L., and Overhage, J. (2024). The role of exopolysaccharides Psl and Pel in resistance of Pseudomonas aeruginosa to the oxidative stressors sodium hypochlorite and hydrogen peroxide. Microbiol. Spectr. *12*, e0092224.

50. Katharios-Lanwermeyer, S., Koval, S.A., Barrack, K.E., and O'Toole, G.A. (2022). The diguanylate cyclase YfiN of Pseudomonas aeruginosa regulates biofilm maintenance in response to peroxide. J. Bacteriol. *204*, e0039621.

51. Christensen, G.D., Simpson, W.A., Younger, J.J., Baddour, L.M., Barrett, F.F., Melton, D.M., and Beachey, E.H. (1985). Adherence of coagulase-negative staphylococci to plastic tissue culture plates: a quantitative model for the adherence of staphylococci to medical devices. J. Clin. Microbiol. *22*, 996–1006. https://doi.org/10.1128/jcm.22.6.996-1006.1985.

52. Gomes, R.N., Borges, I., Pereira, A.T., Maia, A.F., Pestana, M., Magalhães, F.D., Pinto, A.M., and Gonçalves, I.C. (2018). Antimicrobial graphene nanoplatelets coatings for silicone catheters. Carbon *139*, 635–647. https://doi.org/10.1016/j.carbon.2018.06.044.

53. Liao, S., Zhang, Y., Pan, X., Zhu, F., Jiang, C., Liu, Q., Cheng, Z., Dai, G., Wu, G., Wang, L., et al. (2019). Antibacterial activity and mechanism of silver nanoparticles against multidrug-resistant Pseudomonas aeruginosa. Int. J. Nanomedicine *14*, 1469–1487.

54. Jensen, P.Ø., Briales, A., Brochmann, R.P., Wang, H., Kragh, K.N., Kolpen, M., Hempel, C., Bjarnsholt, T., Høiby, N., and Ciofu, O. (2014). Formation of hydroxyl radicals contributes to the bactericidal activity of ciprofloxacin against Pseudomonas aeruginosa biofilms. Pathog. Dis. *70*, 440–443.

55. Khakimova, M., Ahlgren, H.G., Harrison, J.J., English, A.M., and Nguyen, D. (2013). The stringent response controls catalases in Pseudomonas aeruginosa and is required for hydrogen peroxide and antibiotic tolerance. J. Bacteriol. *195*, 2011–2020.

56. Ugurlu, A., Karahasan Yagci, A., Ulusoy, S., Aksu, B., and Bosgelmez-Tinaz, G. (2016). Phenolic compounds affect production of pyocyanin, swarming motility and biofilm formation of Pseudomonas aeruginosa. Asian Pac. J. Trop. Biomed. *6*, 698–701. https://doi.org/10.1016/j.apjtb.2016.06.008.

57. He, X., Han, B., Wang, R., Guo, Y., Kao, R.Y.T., Li, H., Sun, H., and Xia, W. (2023). Dual-action gallium-flavonoid compounds for combating Pseudomonas aeruginosa infection. RSC Chem. Biol. *4*, 774–784.

58. Honselmann genannt Humme, J., Ossowicz-Rupniewska, P., Jurkiewicz, M., Gano, M., Dubrowska, K., Augustyniak, A., Janus, E., Mijowska, E., Favier, L., and Rakoczy, R. (2024). The Comparison of Typical Organic Solvents and Ionic Liquid for More Environmentally and User-Friendly Pyocyanin Extraction. Ind. Eng. Chem. Res. *64*, 781–787.

59. Pires, D., Sillankorva, S., Faustino, A., and Azeredo, J. (2011). Use of newly isolated phages for control of Pseudomonas aeruginosa PAO1 and ATCC 10145 biofilms. Res. Microbiol. *162*, 798–806. https://doi.org/10.1016/j.resmic.2011.06.010.

60. Li, S., She, P., Zhou, L., Zeng, X., Xu, L., Liu, Y., Chen, L., and Wu, Y. (2020). High-Throughput Identification of Antibacterials Against Pseudomonas aeruginosa. Front. Microbiol. *11*, 591426. https://doi.org/10.3389/fmicb.2020.591426.

61. Cruz, C.D., Shah, S., and Tammela, P. (2018). Defining conditions for biofilm inhibition and eradication assays for Gram-positive clinical reference strains. BMC Microbiol. *18*, 173. https://doi.org/10.1186/s12866-018-1321-6.

62. Kirchner, S., Fothergill, J.L., Wright, E.A., James, C.E., Mowat, E., and Winstanley, C. (2012). Use of artificial sputum medium to test antibiotic efficacy against Pseudomonas aeruginosa in conditions more relevant to the cystic fibrosis lung. J. Vis. Exp. e3857. https://doi.org/10.3791/3857.

63. Scherbakova, A., Rykova, V., Danilova, K., Solovyev, A., and Egorova, D. (2020). Extracellular RNA Isolation from Biofilm Matrix of Pseudomonas aeruginosa. Bio-Protocol *10*, e3810. https://doi.org/10.21769/BioProtoc.3810.

64. Schmittgen, T.D., and Livak, K.J. (2008). Analyzing real-time PCR data by the comparative CT method. Nat. Protoc. *3*, 1101–1108.

STAR★METHODS

KEY RESOURCES TABLE

REAGENT or RESOURCE	SOURCE	IDENTIFIER
Bacterial and virus strains		
Pseudomonas aeruginosa PAO1	Gift from another lab	N/A
Chemicals, peptides, and recombinant proteins		
Luria-Bertani (LB)	Beyotime	Cat# ST158
Tryptic Soy Agar (TSA)	Sigma-Aldrich	Cat# 22091
Tryptic Soy Broth (TSB)	Sigma-Aldrich	Cat# T8907
Dulbecco's modified Eagle's medium (DMEM)	Gibco	Cat# 11965-092
Fetal Bovine Serum (FBS)	Gibco	Cat# 10270106
Penicillin and streptomycin	Gibco	Cat# 15140-122
Hydrazine monohydrate	Sigma-Aldrich	Cat# 207942
Dithiothreitol (DTT)	Aladdin	Cat# D265376
Tris(2carboxyethyl) phosphine (TCEP)	Energy chemical	Cat# W830194
2-mercaptoethanol	Bio-Rad	Cat# 1610710
Pyocyanin	Sigma-Aldrich	Cat# P0046
Sodium ascorbate	Aladdin	Cat# S105025
Sodium sulfite	Aladdin	Cat# S572396
hydroxylamine (HA)	Macklin	Cat# H828371
2-hydroxylethyl hydrazine (HEH)	Aladdin	Cat# H113414
3-amino-3-azabicyclo[3.3.0]octane (AAO)	Aladdin	Cat# A124225
1-Aminopiperidine (AP)	Aladdin	Cat# A113934
1-amino-4-methylpiperazine (AMP)	Aladdin	Cat# A151724
2-hydrazinopyridine (HPy)	Aladdin	Cat# H133458
D-Glucose	Macklin	Cat# D810594
L-glucose	Bide	Cat# 54827
Crystal violet	Sigma-Aldrich	Cat# C0775
2′,7′-dichlorofluorescin diacetate (DCFDA)	Aladdin	Cat# H131224
Resazurin sodium salt	Thermo Fisher	Cat# B21187.03
XTT sodium salt	Aladdin	Cat# X100982
TRIzol®	Invitrogen	Cat#15596018
Critical commercial assays		
LIVE/DEAD™ BacLight™ Bacterial Viability Kit	Thermo Fisher	Cat# L7012
Cell Counting Kit-8	Beyotime	Cat# C0039
PrimeScript™ RT reagent Kit	Takara	Cat# RR047A
TB Green® Premix Ex Taq	Takara	Cat# RR420A
Experimental models: Cell lines		
Human Embryonic Kidney (HEK293T) cells	ATCC	N/A

EXPERIMENTAL MODEL AND STUDY PARTICIPANT DETAILS

Bacterial strain

All experiments were performed with *Pseudomonas aeruginosa* PAO1, which was a gift from Prof. Yongxin Li from the University of Hong Kong. This is a standard laboratory-adapted strain. Bacteria were cultured in Luria-Bertani (LB) medium for overnight growth or Tryptic Soy Broth (TSB) for biofilm assays at 37 °C. Sex is not a relevant biological variable for this bacterial model.

Cell line

Human Embryonic Kidney (HEK293T) cells (ATCC® CRL-3216™) were purchased from ATCC used for cytotoxicity assays. The cells were cultured in Dulbecco's Modified Eagle's Medium (DMEM) supplemented with 10% Fetal Bovine Serum (FBS) and 1% penicillin/streptomycin at 37 °C in a 5% CO_2 incubator. Cell line was authenticated by morphology and growth characteristics; no mycoplasma contamination was detected by PCR assay.

METHOD DETAILS

Agar growth assay for selected reagents against *P. aeruginosa* biofilm

A 3 mL *P. aeruginosa* PAO1 LB culture was initiated from a colony on a LB agar plate and grown overnight (16-24 hours) at 37 °C with shaking at 220 rpm. Following the overnight incubation, the culture was diluted with LB liquid medium to achieve the desired optical density (OD_{600} = 0.1) for initiating experiments. Subsequently, tryptic soy agar (TSA) medium was prepared in 6-well plates. Various concentrations of selected reagents (0, 6.25 mM, 12.5 mM, 25.0 mM, 50.0 mM, and 100.0 mM) were added, each at 20 μL, to 2 mL of TSA medium and mixed thoroughly. This mixture was then transferred to the 6-well plates and allowed to solidify. After preparing the plates, 5 μL of the diluted *P. aeruginosa* PAO1 culture (OD_{600} = 0.1) was applied to each agar plate. The plates were then incubated at room temperature for 72 h in the dark to form mature biofilm, and the resulted colony-based biofilm was photographically recorded for comparison.

Antimicrobial activity test for selected reagents against *P. aeruginosa*

Overnight cultures of *P. aeruginosa* PAO1 were prepared as described above and diluted in fresh LB broth to an OD_{600} of 0.1. Aliquots (20 μL) of the standardized suspension were inoculated into 2 mL LB broth containing test reagents at final concentrations of 0, 6.325, 12.5, 25.0, 50.0, or 100.0 mM. Cultures were incubated at 37 °C with shaking at 220 rpm for 24 h. Bacterial growth was quantified by measuring OD_{600} using a microplate reader, with untreated cultures serving as controls.

Quantitation of biofilm biomass

This assay was adapted from methods described in previous studies.[51,52] A 3 mL LB culture was initiated from a single colony on a LB agar plate. The culture was grown overnight (16–24 h) at 37 °C with shaking at 220 rpm. After the overnight incubation, it was diluted with LB liquid medium to an optical density (OD_{600}) of 0.1 to start the experiments. For the inhibition assay, 10 μL of the diluted bacterial solution was inoculated into each well of a 96-well plate containing 100 μL of various concentrations of reagents in Tryptic Soy Broth (TSB) medium. The plates were then incubated at 37 °C for 2 days. For the eradication assay, 10 μL of the diluted bacterial solution was first seeded into each well of a 96-well plate containing 100 μL of TSB medium and incubated at 37 °C for 2 days to allow biofilm formation. Following this, each well was treated with 100 μL of different concentrations of reagents in TSB medium for another 2 days. For post treatment bacteria regrowth assay, 10 μL of the diluted bacterial solution was inoculated into each well for the inhibition and eradication treatments were carried out as mentioned above accordingly, but treatments were applied continuously for up to 7 days. After treatment, the supernatant was removed, and each well was washed three times with 200 μL of PBS. The biofilms were then fixed with 100 μL of methanol for 15 min, after which the methanol was replaced with 200 μL of 0.1% crystal violet and left to stain at room temperature for 15 min. The wells were then washed three times with 200 μL of sterile water to remove excess dye. Once air-dried, the stained biofilms were redissolved by adding 200 μL of 30% acetic acid to each well. The absorbance at 595 nm was measured using a microplate reader to quantify the biofilms.

DCFDA assay for biofilm ROS quantification

Reactive oxygen species (ROS) levels in biofilms were determined using DCFDA (2',7'-dichlorofluorescin diacetate) as described previously with minor modifications.[53–55] Biofilms obtained from the inhibition and eradication assays (Section quantitation of biofilm biomass) were gently washed three times with 200 μL PBS, followed by staining with 200 μL DCFDA (10 μM) for 30 min at 37 °C in the dark. The probe solution was then carefully removed to avoid disturbing the biofilm structure, and wells were washed 2–3 times with sterile PBS to remove excess and unbound dye. Fluorescence intensity of the oxidized product (DCF) was measured using a fluorescence spectrophotometer at an excitation wavelength of 485 nm and an emission wavelength of 535 nm.

Live/Dead BacLight viability assay

The viability of biofilm-embedded cells was determined using the LIVE/DEAD™ BacLight™ Bacterial Viability Kit (Thermo Fisher Scientific) according to the manufacturer's instructions, with minor modifications. Biofilms obtained from inhibition or eradication assays (Section quantitation of biofilm biomass) were treated with the $MBIC_{50}$ or $MBEC_{50}$ concentrations of each hydrazine derivative (Table S1) in 20 mm glass-bottom confocal dishes. Following treatment, supernatants were removed, and biofilms were gently washed three times with 1 mL PBS to eliminate non-adherent cells. A staining solution was prepared by mixing 3 μL SYTO 9 and 3 μL propidium iodide in 1 mL deionized water. 200 μL of this solution were added directly to the biofilm, and dishes were incubated for 20 min at room temperature in the dark. Samples were then rinsed with deionized water to remove excess stain, residual liquid was carefully aspirated, and 1 mL deionized water was added to prevent drying prior to imaging.

Quantification of pyocyanin levels in biofilms treated with hydrazine

Pyocyanin (PYO) levels in wild-type *P. aeruginosa* biofilms were quantified following established protocols with modifications.[56–58] Biofilms were generated in 6-well plates under eradication assay conditions as described in Section quantitation of biofilm biomass, and treated with hydrazine hydrate (HZ) at 6.3, 12.5, 25.0, 50.0, or 100.0 mM, with untreated wells serving as controls. After 48 h of treatment, supernatants and biofilms were processed separately. For supernatants, 2 mL of culture medium was collected, and OD_{600} was measured. Chloroform (600 μL) was added, and the mixture was vortexed until the lower organic phase turned blue. The upper aqueous phase was discarded, and 200 μL of 0.2 N HCl was added to the chloroform phase. After vertexing, the upper aqueous layer turned red. The tubes were left to stand until phase separation was complete. For biofilms, residual biofilm in the wells was resuspended in TSB by sonication, and OD_{600} was measured. Chloroform (300 μL) was added, and the extraction was performed as described above, using 100 μL of 0.2 N HCl for the final step. In both cases, the upper aqueous layer containing pyocyanin was collected, and absorbance was measured at 520 nm. Pyocyanin levels were normalized to bacterial density (OD_{600}) for comparative analysis.

XTT and resazurin assays for biofilm metabolic activity

Biofilm metabolic activity was quantified using XTT and resazurin assays following established protocols with modifications.[59–62] Biofilms were prepared under inhibition and eradication assay conditions as described in Section quantitation of biofilm biomass, with treatments consisting of the tested hydrazine derivatives at 0, 6.3, 12.5, 25.0, 50.0, or 100.0 mM. For the XTT assay, 200 μL of XTT working solution (0.2 mg/mL XTT supplemented with 0.02 mg/mL PMS) was added to each well, and plates were incubated for 3 h at 37 °C in the dark. Absorbance was then measured at 490 nm using a microplate reader. For the resazurin assay, 100 μL of resazurin working solution (0.02 mg/mL in PBS) was added to each well, and plates were incubated for 2 h at 37 °C in the dark. Fluorescence was recorded at an excitation wavelength of 550 nm and an emission wavelength of 590 nm using a fluorescence spectrophotometer.

Cytotoxicity assay

HEK293T cells were seeded in a 96-well plate at a density of 10^4 to 10^5 cells per well, using 100 μL of DMEM medium supplemented with 10% FBS and 1% penicillin/streptomycin. The cells were cultured in a CO_2 incubator at 37 °C for 24 h to allow for adhesion and growth. Following this initial incubation, various concentrations of reagents were added to the wells. The plate was then returned to the incubator and allowed to incubate for an additional 2 days to assess the cellular response to the reagents. After the 48-hour incubation, the supernatants of the wells were carefully removed and replaced with 100 μL of fresh DMEM containing 10% FBS, 1% penicillin/streptomycin, and 10% CCK-8 solution in each well. This working solution allowed for the assessment of cell viability. The plate was then incubated for an additional 1 h in the CO_2 incubator at 37 °C and gently mixed on an orbital shaker for 1 min. Finally, the absorbance was measured at 456 nm using a microplate reader to quantify the cell viability.

RNA extraction

For RNA isolation, *P. aeruginosa* PAO1 was cultured under both planktonic and biofilm conditions. For planktonic growth, the overnight culture was then diluted to an optical density of $OD_{600} = 0.1$ in LB medium and further incubated at 37 °C with shaking at 220 rpm for 18–20 h to maintain free-living growth. In contrast, biofilm cultures were established by inoculating the same diluted suspension ($OD_{600} = 0.1$) into 3 mL LB medium in 15 mL Falcon tubes, followed by static incubation at 37 °C for 18–20 h, which allowed for biofilm formation. Total RNA was extracted using TRIzol® reagent following a modified standard protocol.[63] Briefly, bacterial pellets were resuspended in 1 mL TRIzol and homogenized by vigorous pipetting. Phase separation was achieved by adding 0.2 mL chloroform, followed by vortexing for 15 s and incubation at room temperature for 10 min. After centrifugation at 12,000 × g for 15 min at 4 °C, the aqueous phase containing RNA was carefully transferred to a new tube, and RNA was precipitated by adding 0.5 mL isopropanol per 1 mL TRIzol used. The mixture was incubated for 10 min at room temperature and centrifuged at 12,000 × g for 10 min at 4 °C. The resulting RNA pellet was washed with 1 mL of 75% ethanol, vortexed briefly, and centrifuged at 7,500 × g for 5 min at 4 °C. Ethanol was discarded, and the pellet was air-dried for 5–10 min, taking care to avoid over-drying. Finally, RNA was dissolved in 20–50 μL RNase-free water or TE buffer and stored at −80 °C until further analysis.

qRT-PCR

Total RNA obtained from planktonic and biofilm cultures was treated with TURBO™ DNase (Invitrogen) at 37 °C with shaking at 300 rpm for 30 min to remove genomic DNA, followed by Proteinase K digestion at 37 °C with shaking at 300 rpm for 15 min to eliminate residual proteins. The purified RNA was subsequently reverse transcribed into cDNA using the PrimeScript™ RT reagent Kit (Takara) according to the manufacturer's protocol. qRT-PCR was performed on a Bio-Rad CFX96 Touch Real-Time PCR Detection System using TB Green® Premix Ex Taq™ (Tli RNase H Plus, Takara). Primer sequences for target genes are provided in Table S2. Amplification was conducted under the following cycling conditions: initial denaturation at 95 °C for 3 min, followed by 39 cycles of denaturation at 95 °C for 10 s and annealing/extension at 63 °C for 30 s.[48] A final denaturation step at 95 °C for 5 s was applied before performing melting curve analysis to verify amplification specificity. The ribosomal protein gene rpsL served as the internal reference for normalization. Relative expression levels of target genes were calculated using the comparative Ct ($2^{-\Delta\Delta Ct}$) method, based on normalized threshold cycle (Cq) values.[64]

QUANTIFICATION AND STATISTICAL ANALYSIS

All experiments were performed in triplicate (n=3) unless otherwise stated. Data were presented as mean ± standard deviation (SD), as specified in the figure legends. Statistical analyses were performed using GraphPad Prism software. For quantitative assays such as crystal violet, DCFDA, XTT, and resazurin, the value 'n' represents the number of independent biological replicates. For the Live/Dead BacLight assay, viability was quantified using ImageJ software from three independent experimental images. The relative gene expression in qRT-PCR was calculated using the Ct ($2^{-\Delta\Delta Ct}$) method, error bars define the variation around the mean of the replicates, *$p < 0.05$ were used to determine the statistical significance of differences.